chemically generated CdS particles.

Conclusion

The most significant accomplishment of the present work has been the demonstration of electrochemical generation of CdS particles in the matrices of conducting polymers. Advantage has been taken of ion incorporation dynamics under potential control to introduce the necessary precursors into the polymer matrices. Thus, Cd^{2+}, incorporated into negatively charged PPy/PSS^- polymer composites, has been converted to CdS by the subsequent introduction by HS^- ions. Alternatively, HS^- ions, introduced into positively charged PPy, provided a useful precursor for attracting Cd^{2+} and for the subsequent CdS formation. The EQCM has played a pivotal part in the optimization of the required experimental conditions. Although at present we could only produce irregular CdS particles, we are confident that judicious improvements of the experimental methodology will allow the formation of size-controlled and dimensionally reduced semiconductor particles in the matrices of conducting polymers.

Acknowledgment. Support of this work by a grant from the Department of Energy is gratefully acknowledged. M.H. thanks the National Science Foundation for a Research Opportunity Award. D.Y. is the holder of a Chaim Weizmann Postdoctoral Fellowship for Scientific Research.

Registry No. PSS^-Na^+, 9080-79-9; CdS, 1306-23-6; Cd, 7440-43-9; pyrrole (homopolymer), 30604-81-0.

Crystallization Behavior of Xerogels in a Cr_2O_3-Doped SiO_2–Al_2O_3–ZnO System

W. Nie and G. Boulon*

Laboratory of Physical Chemistry and Luminescent Materials, University Claude Bernard Lyon I, UA CNRS 442, 69622 Villeurbanne, France

C. Mai and C. Esnouf

GEMPPM, INSA of Lyon, UA CNRS 341, 69621 Villeurbanne, France

Xu Runjuan and J. Zarzycki

Laboratory of Sciences of Vitreous Materials, UA 1119, University of Montpellier 2, 34060 Montpellier Cedex 1, France

Received May 9, 1991. Revised Manuscript Received November 12, 1991

Nucleation, crystallization, and characterization of nanocrystallites and xerogels of the Cr_2O_3-doped SiO_2–Al_2O_3–ZnO system have been studied. The techniques used are X-ray diffraction, small-angle X-ray scattering, transmission electron microscopy, optical absorption, and laser spectroscopy techniques.

Introduction

In previous papers we have explained our approach to research on nucleation induced in gahnitelike glasses or xerogels by chromium oxide.[1-3] Indeed, the chromium element is both an excellent nucleating agent and a good structural fluorescent probe so that we may apply to such systems scattering techniques and laser spectroscopy, which are complementary techniques in the characterization of materials. The first part of our program dealt with glasses of SiO_2–Al_2O_3–MgO and SiO_2–Al_2O_3–ZnO[2] systems. In the present work we will present new data on the SiO_2–Al_2O_3–ZnO system synthesized by the sol–gel route, keeping the same initial compositions as that of glasses synthesized by the standard method. Under different heat treatments from 50 to 1000 °C, we follow the transitions sol–gel → glass → glass–ceramic. In addition to understanding the nucleation mechanism, another motivation is to improve our knowledge on the optical properties of gels. To this end, several xerogel samples were prepared with various proportions of components and were analyzed by X-ray diffraction, small angle X-ray scattering (SAXS), transmission electron microscopy (TEM), energy dispersive X-ray spectroscopy, optical absorption, and laser spectroscopy techniques. We will give the main structural results in the continuous transformation of the samples under thermal treatment from low to high temperature.

Experimental Section

The preparation of xerogels and characterization methods are described in ref 3. SAXS measurements were carried out using a special camera mounted on a Rigaju rotating anode (12 kW) X-ray generator. A one-dimension position-sensitive detector and a multichannel analysis system connected to a microcomputer allowed rapid measurements. A pointlike slit conditions with an irradiated cross section of about 1 mm^2 was used. This type of collimation avoided mathematical desmearing. This is essential to improve the accuracy of the experimental results in order to study the fractal behavior. Both the sameple and the X-ray beam of wavelength 1.54 Å were in vacuum to reduce air scattering. Scattering curves were obtained in the range of vector $\mathbf{q} = (4\pi \sin \vartheta/\lambda)$ from 10^{-2} to 5×10^{-1} $Å^{-1}$. The parasitic scattering from holder and slits was subtracted from the experimental SAXS intensity.

TEM observations were performed on a 200 CX Jeol microscope. Thin samples were prepared by a crushing technique. The glass powder was deposited on carbon film from a suspension of

(1) Ponçon, V.; Bouderbala, M.; Boulon, G.; Lejus, A. M.; Reisfeld, R.; Buch, A.; Ish-Shalom, M. *Chem. Phys. Lett.* **1986**, *130*, 444.
(2) Ponçon, V.; Nie, W.; Boulon, G. *Eur. J. Solid State Inorg. Chem.* **1989**, *26*, 53-70.
(3) Nie, W.; Boulon, G.; Maï, C.; Esnouf, C.; Rundjuan, Xu; Zarzycki, J. *J. Non-Cryst. Solids* **1990**, *121*, 282-287.

0897-4756/92/2804-0216$03.00/0 © 1992 American Chemical Society

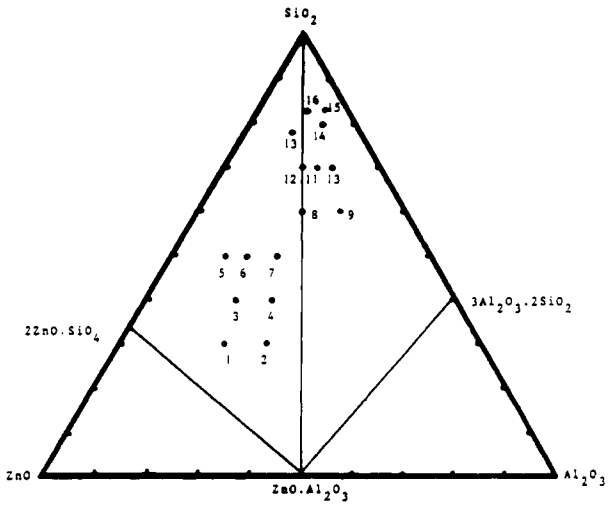

Figure 1. Domain of the compositions studied.

Table I. Results of Heat Treatments

sample	temp, °C	time, h	appearance[a]	crystalline phases[b]
8	800	4	O	G
9	800	4	O	G, M
10	800	1–20	T	G, M
	1000	2	T	G, M
11	800	1–20	T	G, M
	1000	2–5	T	G, M
12	800	1–4	T	G
		20	T	G, Q
	1000	2–5	T	G, Q
13	800	1–20	TL	G, Q
	1000	2	O	G, Q, W
14	800	1–20	T	G, M
	1000	2–5	T	G, M
15	800	1–20	T	G, M
	1000	2–5	T	G, M
16	800	1–4	T	G
		20	T	G, Q
	1000	2	T	G, Q

[a] Key: O, opaque; T, transparent; TL, translucent. [b] Key: G, gahnite; M, mullit; W, willemite; Q, quartz.

particles in methanol and dried. Both dark fields and selected area diffusion methods were used.

Absorption spectra were recorded with a Varian 2300 automatic spectrophotometer. The samples can be studied from 4.2 K to room temperature using a cryogenic system especially adapted to the spectrophotometer.

Laser spectroscopy techniques were performed with a tunable pulsed dye laser. We used both site selection spectroscopy and time-resolved spectroscopy. A Quantel Nd:YAG laser (repetition rate 10 Hz, time constant 15 ns, line width 0.1 cm^{-1}) with a KDP frequency doubler (532 nm) was used to pump dye lasers.

Results and Discussion

XRD Patterns. Figure 1 shows the domain of compositions studied. For compositions 1 to 7, crystallization occurred below 700 °C; the crystallized phases were gahnite ($ZnAl_2O_4$) and willemite (Zn_2SiO_4).

The results for compositions 8 to 16 after heat treatments at 800 and 1000 °C are presented in Table I. Note that for compositions containing less than 70 mol % SiO_2, no transparent gels could be obtained after heat treatments. When the ZnO/Al_2O_3 ratio is increased to 1.5 (sample 13), the gels become opaque even though SiO_2 content exceeds 70 mol %.

The temperature at which crystallinity occurs appears to be related to the SiO_2 concentration. For compositions containing more than 60 mol % SiO_2, no evidence of crystallization is observed after heat treatment for 4 h at 700 °C. At 800 °C crystallization occurred abruptly.

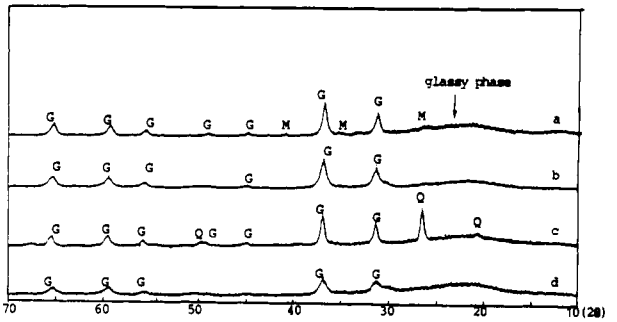

Figure 2. X-ray diffraction spectra of the samples 11 and 16 at 1000 °C for 2 h: (a) composition 11; (b) composition 11 + 2 mol % ZrO_2; (c) composition 16; (d) composition 16 + 2 mol % ZrO_2.

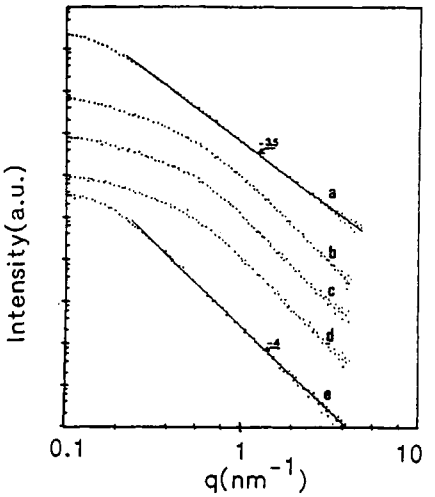

Figure 3. SAXS curves of xerogels KCR1 heat-treated at (a) 50 °C, (b) 700 °C, (c) 800 °C, and (d) 1000 °C and (e) crystallized glass.

It was also observed that mullite and gahnite appeared simultaneously after 1 h at 800 °C, traces of quartz appearing only after 4 h (except for sample 13). For all samples studied, coexistence of mullite and quartz seems to be inhibited.

For compositions with ZnO/Al_2O_3 molar ratio 1.0 or approximately 1 (samples 8, 12, and 16) crystallization behavior varied with the SiO_2 concentration. For sample 8, gahnite was the only crystalline phase; increase of the SiO_2 content leads to the appearance of quartz (samples 13 and 16). For compositions with 70 mol % SiO_2 (samples 10–12), quartz decreases and mullite increases with the decrease of the ZnO/Al_2O_3 ratio.

To inhibit the crystallization of phases other than gahnite and conserve the transparency of the samples, ZrO_2 was introduced (2 mol %) into compositions 11, 15, and 16.

Figure 2 shows the effect of ZrO_2 introduced into compositions 11 and 16. Up to 1000 °C there was no evidence of formation of phases other than gahnite, the sample remaining transparent and glasslike. ZrO_2 crystals did not appear.

It is likely that these materials can be considered as glass–ceramics, where the gahnite phase dispersed in a glass matrix was preferentially precipitated on ZrO_2 nuclei. However in the following work we will only analyze samples without any ZrO_2.

SAXS Analysis. The experimental results are grouped into (i) nonnucleated xerogel, sample dried at 50 °C (noted a), and (ii) nucleated xerogel, sample heat-treated 2 h at 700 °C (b) or 2 h at 800 °C (c) or 2 h at 1000 °C (d).

Figure 3 shows the experimental SAXS curves plotted as log $I(q)$ versus long q for the different samples. The dissimilarity of curves a and curves b–d indicates that the nonnucleated and the nucleated xerogels ae structurally different. In nonnucleated xerogels the scattered intensity is proportional to $q^{-3.5\pm0.1}$, where the uncertainty of the exponent was estimated from the reproductibility of the scattering curves for a wide interval of q. This kind of curve can be explained as being the result of the scattering from a fractal structure.[4-7]

It is necessary to distinguish between bulk and surface scattering. For mass or volume fractal objects the scattered intensity $I(q)$ obeys a power-law < 3 is the fractional or fractal dimension.[4] The scattering from mass fractals is discussed in detail by Schaeffer and Keefer.[5]

For the surface fractal, Bale and Schmidt[6] have given the following formula

$$I(q) \propto q^{-(6-D_s)} \quad (1)$$

where D_s is the surface fractal dimension. Several aspects of surface scattering should be noted. If $D_s = 2$ as for a smooth surface, the scattered intensity decays as q^{-4}. This behavior is commonly called Porod's law and thus eq 1 is a generalization of Porod's law. If $2 < D_s < 3$ as for fractal surfaces, Porod slopes between −3 and −4 are expected.

(a) Nonnucleated Samples. Experimental results for nonnucleated samples show that the xerogel contains pores which are bounded by surfaces with a fractal dimension $D_s = 2.5$.

The scattering data can alternately be considered as the result of submicroscopic pores or particles with a power-law size distribution. The scattered intensity calculated from such a law[7] is proportional to $q^{-(6-D)}$ as given by eq 1. Avnir et al.[8] have shown that pores bounded by fractal surfaces can explain the absorption data for several absorbents. Their results suggest that such fractal–pore systems may be more common than was previously suspected. We believe that systems of pores with a power-law dimension distribution scatter in essentially the same way for large q as pores with boundaries so rough that they can be described by fractal surfaces.

In this case, thermoporometry measurements performed on several samples effectively show pores characterized only by small sizes <1 nm.

(b) Nucleated Samples. For nucleated samples denoted as b, c, and d in Figure 6, the SAXS curves are more complex. At large q the data are proportional to q^{-4} whereas at smaller q the scattered intensity varies continuously and no power-law regimes are clearly seen. Interpretation of such a system would be difficult due to the presence of crystalline particles. It should be mentioned that in equivalent nucleated glasses the slope of the curve is close to 4, as expected, without any evidence of fractional power law. The strong difference between the behavior of xerogels (b–d) and glasses (e) can easily be seen in Figure 3.

The crystalline particle size distribution can be calculated from the scattering curves using the correlation function

$$\gamma(t) = \int_R f_v(D)\, \gamma_D(r)\, dD \quad (2)$$

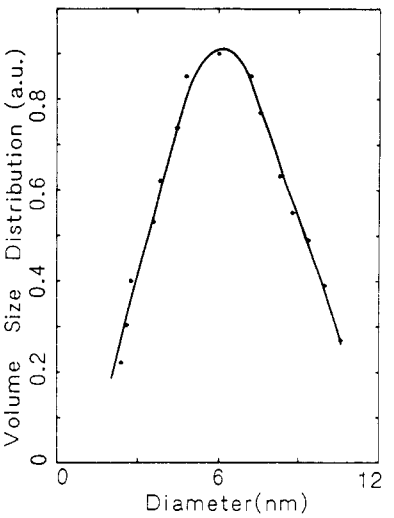

Figure 4. Volume size distribution of particles in xerogel KCR1 heated for 2 h at 800 °C.

Table II. Sizes of Nanocrystallites

T, °C	diameter of the bigest nanocrystallites (result of TEM), nm	av diameter of nanocrystallites (result of SAXS), nm
KCR 2		
700	5 ± 0.5	6.6 ± 0.2
600	11 ± 0.5	7.0 ± 0.2
1000	21 ± 0.2	10.4 ± 0.2
KCR 1		
50	8[a] ± 0.5	
700	4 ± 0.5	
800	10 ± 0.5	
gel B		
1000	13.5 ± 0.5	

[a] Formation of nitrates in the initial composition.

where $f_v(D)$ is the volume size distribution of particles with diameter D. In eq 2 $\gamma_D(r)$ is the correlation function of a spherical particle with diameter D which is given by the relation

$$\gamma_D(r) = 1 - \frac{3r}{2D} + \frac{r^3}{2D^3}$$

$$0 < r < D$$

Solving eq 2 for the $f_v(D)$ yields

$$f_v(D) = (D/3)[\gamma''(D) - D\gamma''(D)] \quad (3)$$

Calculations from eq 3 require values of $\gamma(r)$ up to the third order. A numerical calculation method was used[10] and the validity of the determination of the particle size distribution depends on the sphericity of the particles. Therefore, the morphology of the particles was controlled before any calculation by TEM micrography. Figure 4 shows a field micrograph of the sample heat treated for 2 h at 800 °C. Most particles have nearly cubic shapes so that sizes can only be measured approximately. Table II gives results corresponding to the maximum of the particle size distribution as illustrated in Figure 4. We also give values of the largest size of the nanocrystallites measured directly from TEM in order to compare them with the previous results. Slight discrepancies are noted depending on the selected crystallites observed with a microscope but also depending on the absence of spherical crystallites,

(4) Mandelbrot, B. B. *Fractals Form and Chance*; Friedman: San Francisco, CA, 1987.
(5) Schaefer, D. W.; Keefer, K. D. *Mater. Res. Soc. Symp. Proc.* **1984**, *32*, 1.
(6) Bale, M. D.; Schmidt, P. W. *Phys. Rev. Lett.* **1984**, *53*, 596.
(7) Schmidt, P. W. *J. Appl. Crystallogr.* **1982**, *15*, 567.
(8) Avnir, D.; Farm, D.; Pfeifer, P. *J. Chem. Phys.* **1988**, *79*, 3566.
(9) Donatti, J. R.; Pascal, B.; Renouprez, A. J. *Bull. Soc. Fr. Mineral. Cristallogr.* **1967**, 452.
(10) Maï, C.; Linet, F.; Vigier, G. *Scr. Metall.* **1981**, *15*, 1179.

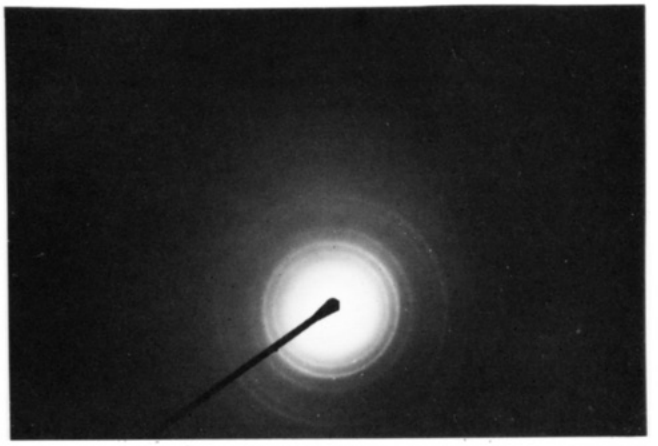

Figure 5. Dark field TEM photographs: (a, top) electron diffraction and (b, bottom) nanocrystallites.

Table III. Lattice Constants a_0 Measured by TEM and the Average Distance d between Al^{3+} and O^{2-} Deduced in the Homothetic Assumption

KCR2

		KCR2			
	$ZnAl_2O_4$	2 h, 1000 °C	2 h, 800 °C	2 h, 700 °C	$ZnCr_2O_4$
a_0, Å	8.0848	8.2098	8.2743	8.3075	8.3275
d, Å	1.915	1.941	1.948	1.961	1.965

KCR1 and Gel B

	$ZnAl_2O_4$	KCR1 2 h, 800 °C	gel B 2 h, 1000 °C	$ZnCr_2O_4$
a_0, Å	8.0848	8.2051	8.0812	8.3275
d, Å	1.915	1.940	1.914	1.965

which is the essential condition to apply the theory.

Diffraction Pattern from TEM. During the nucleation process, the nanocrystallites were systematically controlled. To this end, a thin film reference of microcrystalline aluminum was used in the same experimental conditions as those of xerogel and glass–ceramic samples, that is, conditions on excentricity and fine adjustments of camera length. Figure 5 shows a dark field micrograph of a sample heat-treated 2 h at 800 °C for which the selection aperture takes into account only 10% of the principal diffraction ring. Depending on the heat-treatment conditions, the diffraction patterns can be related to a spinelike structure characterized by an evolutive lattice constant, a_0, from $ZnCr_2O_4$ to $ZnAl_2O_4$. At 800 °C a cubic structure with $a_0 = 8.30$ Å is obtained; this value may be compared with $ZnCr_2O_4$ ($a_0 = 8.3275$ Å), whereas for higher temperatures (1000 °C) the parameter is closer to that of $ZnAl_2O_4$ ($a_0 = 8.0848$ Å). For instance, the measured lattice constants given in Table III are the average values of five experiments corresponding to high intensity reflection usually noted 220, 311, 400, 511, and 440 with estimated errors less than ±0.05 Å. The nucleation process was also characterized by using an energy dispersive X-ray (EDX) spectroscopy associated with 200 CX Jeol TEM.

A comparison between EDX spectra obtained in a region within the glassy matrix without any crystallite and in a large crystallite is shown in Figure 6. It was observed that the presence of chromium can only be detected in crystalline zones when the heating temperature is 1000 °C. Results of TEM and EDX show that nucleation of crystalline phase occurs preferentially at chromium sites. At the beginning of nucleation, $Zn(Cr_xAl_{1-x})_2O_4$ is rich in chromium ($x \simeq 1$) and the parameter measured from the diffraction pattern ($a_0 = 8.30$ Å) is close to that of $ZnCr_2O_4$; at higher temperature, or probably at a longer time for a fixed temperature, the crysalline phases grow richer in aluminum cations and a_0 decreases to 8.0812 Å (xerogel 8–0.15% Cr_2O_3) or 8.2098 Å (xerogel KCR 2–0.5% Cr_2O_3). The strong influence of the initial concentration in chro-

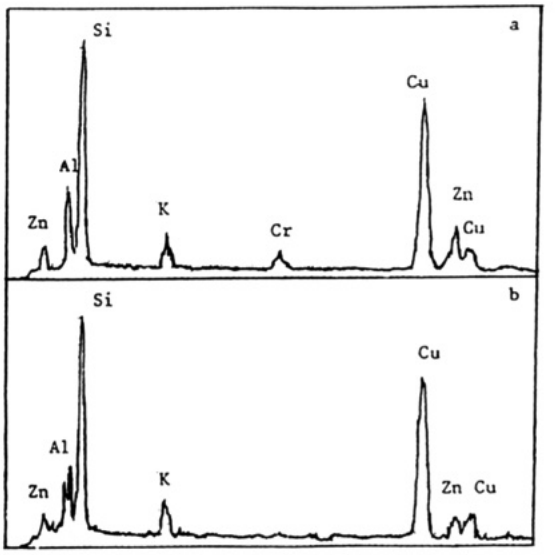

Figure 6. TEM microanalysis: (a) spectrum of a crystallite in xerogel KCR2 heated for 2 h at 1000 °C; (b) spectrum of a thin part without nanocrystallites in xerogel KCR2 heated for 2 h at 1000 °C.

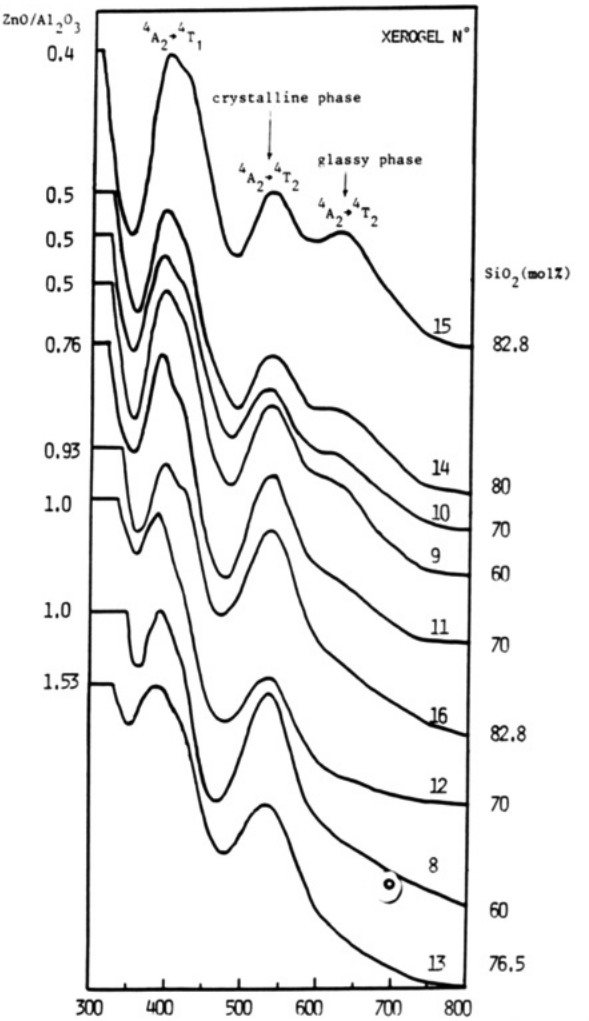

Figure 7. Absorption spectra at room temperature of xerogels which were heated for 2 h at 1000 °C. The ZnO/Al_2O_3 ratio and the percentage of SiO_2 in the initial compositions are noted in the figure.

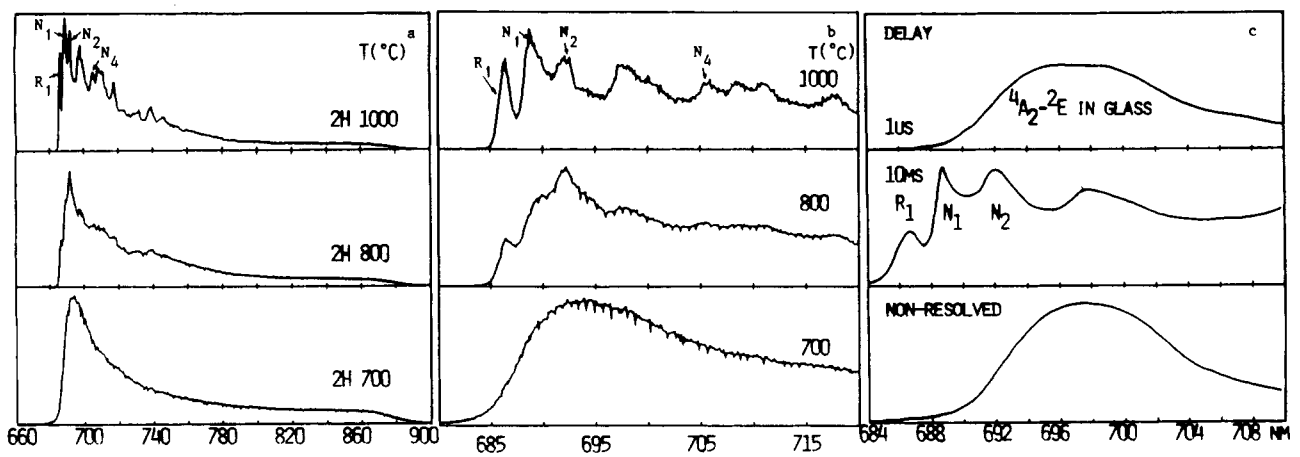

Figure 8. (a) Emission spectra of xerogel KCR1 at 20 K under excitation at 532 nm. (b) Expansion of a. (c) Time-resolved spectra of xerogel KCR1 (2 h, 1000 °C) at 4.4 K under activation at 640 nm.

mium which plays an important role in the average crystallographic distances should be mentioned.

Optical Absorption. We have already shown the advantage of optical absorption in the nucleation studies from glassy phases.[11] The position, bandwidths, and intensities of the well-known $^4A_2 \rightarrow {}^4T_2$ and $^4A_2 \rightarrow {}^4T_1$ transitions of the Cr^{3+} ion can be easily analyzed and compared with spectra of Cr^{3+}-doped glasses or crystals. First of all, after heat treatments, the $Cr^{3+} \rightarrow Cr^{6+}$ transformation occurs, Cr^{6+} being evident by the presence of the strong charge transfer band in the near-UV region at 365 nm. Above 700 °C, this band disappears and Cr^{3+} transitions again appear. At 1000 °C, the highest crystallization temperature we have applied, the absorption spectra are close to those of $Zn(Cr_xAl_{1-x})_2O_4$, depending on the chromium concentration. A finer analysis was made by measuring the $^4A_2 \rightarrow {}^4T_2$ maximum which characterizes the approximative $10Dq$ parameter and, consequently, the mean distance of the Cr^{3+}–O^{2-} ligand as expected by Tanabe and Sugano's theory. For the same crystalline phase, the crystal field strength decreases if the Cr^{3+}–O^{2-} distance increases. In addition, the absorption spectra show an interesting feature on the long wavelength tail; depending on the initial proportions of the system, another broad band was observed close to 630 nm. Several hypotheses have been made regarding the origin of such a tail and even sometimes a structured band. These include Cr^{3+}-doped glasses, Cr^{3+}-doped crystallites of different composition from gahnite, and other ionization states of chromium ions in crystalline or xerogel phase. It can be observed in Figure 7 that the new broad band is much more structured when the ZnO/Al_2O_3 ratio decreases. At first, Cr_2O_3, ZnO, and Al_2O_3 grow gahnitelike nanocrystallites; after saturation of the stoichiometric compound the residual glass seems to be composed of Al_2O_3 and SiO_2 oxides with some traces of Cr_2O_3. It is likely that the residual glassy phase has a composition of mullite ($3Al_2O_3$–$2SiO_2$). The absence of the Cr signal in Figure 6 is due to the low sensitivity of EDX experiments for very low concentration elements. In fact, such a conclusion can only be confirmed with the help of laser spectroscopy techniques, as we demonstrate below.

Laser Spectroscopy Techniques. We have already given a few examples of absorption and fluorescence spectra in ref 11 depending on the structure and the crystal field strength at the Cr^{3+} environment. Our references are Cr^{3+}-doped $ZnAl_2O_4$ and Cr^{3+}-doped glasses from the SiO_2–Al_2O_3–ZnO system[12]. The first vibronic band is associated with the allowed $^4A_2 \rightarrow {}^4T_2$ transition with a maximum at 535 nm in gahnite and 660 nm in glass. By pumping into these two bands (the usual way of exciting Cr^{3+}) two different fluorescence spectra are expected: one corresponding to gahnite and another one corresponding to glass. But it should be mentioned that such an absorption broad band does not belong to any one type of Cr^{3+} site; multisites may occur and the observed absorption band is the envelope of several unresolved broad bands. This means that after simultaneous excitation of multisites by broad-band pumping and relaxation to the lowest vibrational exicted levels, the fluorescence spectra will involve contributions from many kinds of sites. Figure 8 shows the evolution of the emission spectra of KCR1 under thermal treatment from 700 to 1000 °C; the transition from a glasslike xerogel to a glass–ceramic phase can be seen. Whereas two broad bands so-called N(694 nm) and N(IR) characterize the glasslike xerogel in the sample heat-treated 2 h at 700 °C, at higher temperature, the inequivalent Cr^{3+} sites within the gahnite phase can be detected by R, N_1, N^2 (strong crystal field strength) and N(705), N(740), N(IR) (weaker crystal field and consequently higher Cr^{3+}–O^{2-} distance) which are associated with different unperturbed and perturbed sites.[12] According, to the first assumptions, the R lines originate from the transition $^2E \rightarrow {}^4A_2$ of the Cr^{3+} ion substituted at the 16d octahedral site (D_{3d} with a weak trigonal field distortion and spin–orbit interaction) and N_1 and N_2 lines may be assigned to octahedral sites more perturbed by Zn^{2+} vacancies and inversion ratio between Zn^{2+} and Al^{3+} in the first coordination spheres around Cr^{3+} ions. We have shown that the local environment of Cr^{3+} in the N_2 site differs from R and N_1 sites. For instance, the intensity of N_1 line increases with the cooling rate of the sample. In ref 12 we have concluded that the lattice defects occurring close to the N_1 site could be reasonably considered as Zn^{2+} vacancies, as is already expected in zinc compounds. With regard to the N_2 site, it might be connected with the most relevant kind of lattice perturbation such as cation inversion in spinellike structure. The nature of the unequivalent centers can be inferred by the evolution of their relative fluorescence intensities during the nucleation and crystallization processes.

With the laser excitation shifted to 640 nm into the tail of the absorption spectrum, the structure disappears and the emission spectrum characterizes Cr^{3+}-doped glass. For

(11) Boulon, G. *Mater. Chem. Phys.* **1987**, *16*, 301.

(12) Nie, W.; Michel-Calendini, F.; Linarès, C.; Boulon, G.; Daul, C. *J. Lumin.* **1990**, *46*, 177–190.

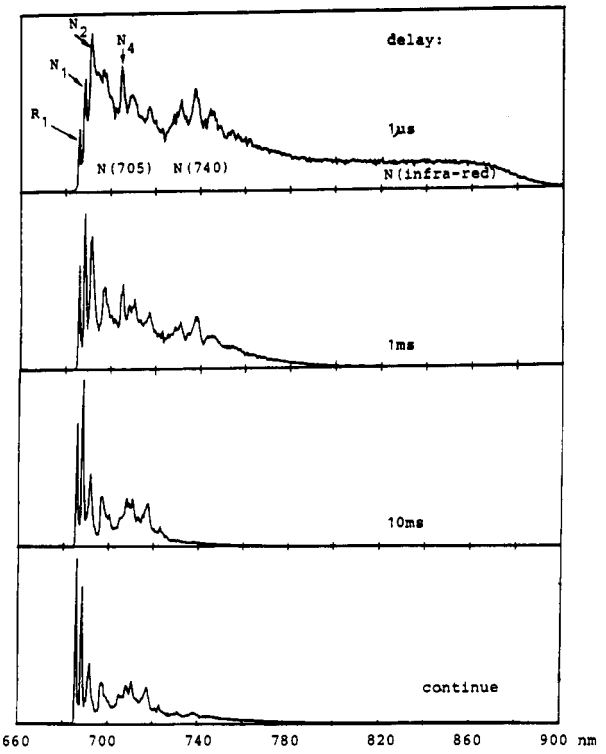

Figure 9. Time-resolved and unresolved emission spectra of $ZnAl_2O_4$:1% Cr at 20 K under excitation at 640 nm.

several samples the residual glass has been identified as mullitelike glass ($3Al_2O_3$–$2SiO_2$) especially by site selection spectroscopy.[3] However, we cannot exclude the presence of a small amount of mullite-type crystalline phase as confirmed by X-ray diffraction patterns. In addition, the time-resolved spectroscopy technique allows us to resolve some traces of the gahnite crystalline phase within the glassy phase, as shown in Figure 8c, due to the excitation of the tail of the broad band with a maximum at 535 nm. Unresolved and short delay spectra (1 μs) are similar to that expected for the $^2E \rightarrow {}^4A_2$ transition of Cr^{3+}-doped glasses, where low symmetry sites give rise to greater transition probabilities and therefore to shorter lifetimes. At longer times (10 ms), the structures of $^2E \rightarrow {}^4A_2$ transitions assigned to R, N_1, and N_2 sites reveal the presence of Cr^{3+} ions in nanocrystallites with higher symmetries. In a general way, we can follow the nucleation mechanisms by optical techniques which are powerful tools to probe local changes in the environment of the Cr^{3+} nucleating agent. Strong differences in the behavior of samples are observed with respect to the initial concentrations of Cr^{3+} ions. On the other hand, resonant selective excitations into ^2E excited levels have been done and will be presented in more detail in a future contribution. As for the previous results,[2] we note the high intensity of strong crystal field strength sites compared to those of weak crystal field sites represented by N(IR)[12] when small concentrations of chromium (0.15% Cr_2O_3) are added to xerogels. There is a great difference between xerogels and glasses; Cr^{3+} ions occupy essentially strong crystal field sites in xerogels whereas they occupy weak crystal field sites in glasses.[2] So the precursor material constituted by xerogel samples leads directly to high crystal field sites. Only a few N(IR) weak crystal field sites are present under 532-nm excitation.

The spectroscopic behavior of the Cr^{3+}-doped $ZnAl_2O_4$ can be analyzed by time-resolved spectroscopy. The different weak crystal field sites N(705), N(740), and N(IR) may be clearly seen only at short delays in Figure 9 due to their small numbers of sites and relatively short lifetimes; in the unresolved spectrum only strong crystal field sites R, N_1, and N_2 and the vibronic lines are recorded. The comparison between Figure 8 and Figure 9 definitely points out the occurrence of Cr^{3+}-doped gahnite nanocrystallites in xerogel-like glass. In addition, the N(IR) broad band in KCR1 belongs to the glassy phase (mullite) rather than crystallites in glass–ceramics; the Cr^{3+} sites from which significant N(705) and N(740) bands originate are more populated than in pure gahnite. As a result, the Cr^{3+} environment of nanocrystallites are slightly perturbed due to the presence of Cr aggregates, and the distribution of different multisites differs from that of Cr^{3+}-doped

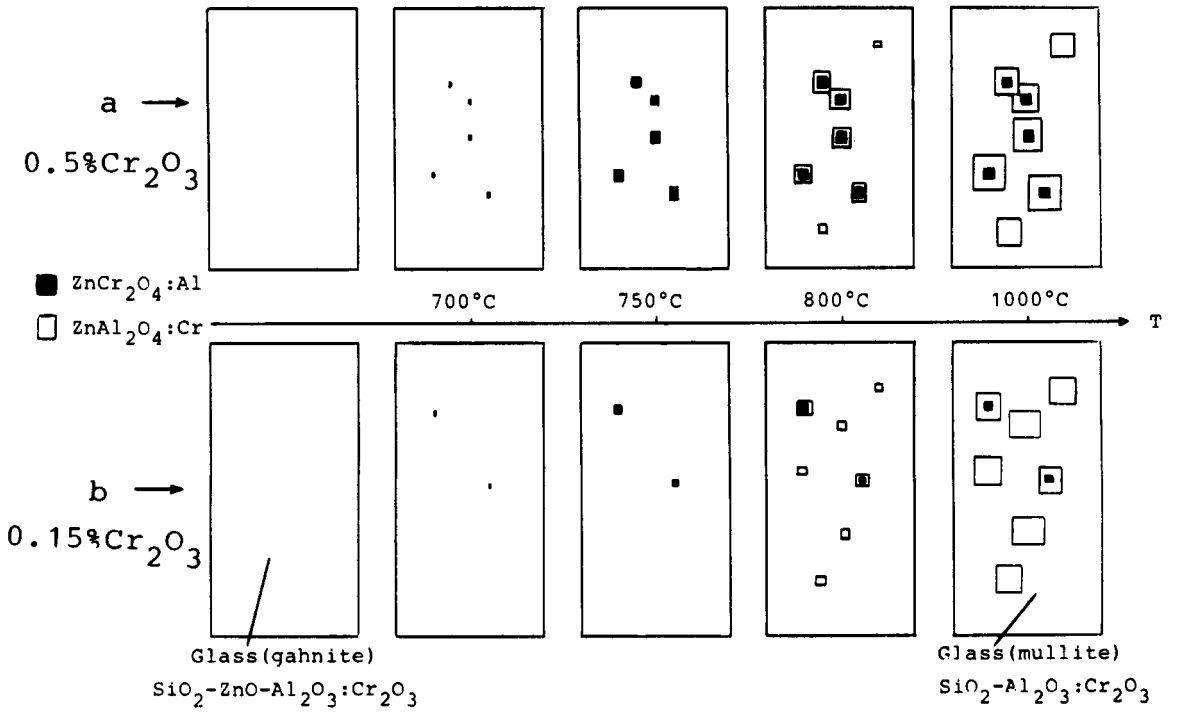

Figure 10. Model of the nucleation and crystallization processes in the SiO_2–ZnO–Al_2O_3–Cr_2O_3 system.

$ZnAl_2O_4$. Hence, at the beginning of the nucleation the nanocrystallites contain $Zn(Al_{2-x}Cr_x)_2O_4$ characterized with x values close to 1, whereas for higher temperatures Cr^{3+}-doped gahnite nanocrystallites are characterized by small x values that overlap with the previous ones. The model of the nucleation and crystallization processes in the SiO_2–ZnO–Al_2O_3–Cr_2O_3 system has been summarized in Figure 10.

We believe that these new results will have large consequences on the interpretation of the spectroscopic properties of Cr^{3+}-doped materials because we now have the possibility of accurately connecting our characterized samples with the emission spectra of both strong and weak crystal field sites.

Conclusion

Xerogels of the SiO_2–Al_2O_3–ZnO system doped by Cr_2O_3 have been synthetized by varying the proportions of the different components. Under heat treatments between 50 and 1000 °C it has been demonstrated that chromium evolves from Cr^{3+}-doped aqueous media at low temperature to Cr^{6+} ions up to 800 °C and then again to Cr^{3+}-doped both in glassy and crystalline phases. X-ray diffraction, small-angle X-ray scattering, and transmission electron microscopy support the conclusion that gahnite-like structure nanocrystallites grow. The average sizes measured in the final glass–ceramic varied from 5 to 21 nm. Such xerogel does not contain pores greater than 1 nm which are bounded by surfaces with fractal dimension $D_s = 2.5$ in nonnucleated samples, whereas nucleated samples cannot be easily explained with a fractal model. The lattice constant changes from $a_0 = 8.30$ Å (close to $ZnCr_2O_4$) at 800 °C to $a_0 = 8.0812$ Å (close to $ZnAl_2O_4$) at 1000 °C. The nucleation appears to form stoichiometric gahnite with the general formula $Zn(Cr_xAl_{1-x})_2O_4$ ($1 > x > 0$). After saturation of ZnO in crystallites, the two other constituents SiO_2 and Al_2O_3 of the xerogel form a mullite glass. The Cr^{3+} fluorescence allows us to detect glassy and crystalline phases and especially the different local environments which evolve during the crystallization mechanism. A direct relation has been made between octahedral crystallographic sites and the presence of lines and emission bands in nanocrystallites. This has important consequences for our understanding of the optical properties of Cr^{3+}-doped gahnite and, also, in a general way, on the properties of luminescent materials owing to well-characterized xerogel samples.

Acknowledgment. This work is supported by Groupement de Recherche (GDR) Verre of CNRS.

Registry No. Al_2O_3, 1344-28-1; ZnO, 1314-13-2; Cr_2O_3, 1308-38-9; gahnite, 1302-75-6.

Effects of Substitution Chemistry in the $KTiOPO_4$ Structure Field

Mark L. F. Phillips,*,† William T. A. Harrison,‡ Galen D. Stucky,‡ Eugene M. McCarron III,§ Joseph C. Calabrese,§ and Thurman E. Gier§

Sandia National Laboratories, Albuquerque, New Mexico 87185; Department of Chemistry, University of California, Santa Barbara, California 93106; and Central Research and Development Department, E. I. du Pont de Nemours, Wilmington, Delaware 19880

Received August 12, 1991

Potassium titanyl phosphate ($KTiOPO_4$, or KTP) is an important nonlinear optical medium whose structure permits a moderate degree of cation mobility. This feature is exploited in the syntheses of $Na_{0.95}K_{0.05}TiOPO_4$ (NaTP), $Ag_{0.85}K_{0.15}TiOPO_4$ (AgTP), and $Na_{0.87}K_{0.13}TiOAsO_4$ (NaTA) from single crystals of KTP and $KTiOAsO_4$ (KTA) through ion exchange at low temperatures, as these compositions do not crystallize in the KTP structure type when prepared from their constituent oxides at high temperatures. All three compounds are orthorhombic, space group $Pna2_1$, with $Z = 8$. For NaTP, $a = 12.611$ (2) Å, $b = 6.2810$ (9) Å, $c = 10.595$ (2) Å; for AgTP, $a = 12.534$ (2) Å, $b = 6.2939$ (9) Å, $c = 10.524$ (1) Å; for NaTA, $a = 12.8884$ (9) Å, $b = 6.4095$ (3) Å, $c = 10.7393$ (6) Å. Crystals of α-$NaTiOPO_4$, the high-temperature polymorph of NaTP, were prepared hydrothermally. This phase crystallizes in the titanite ($CaTiOSiO_4$) structure and is monoclinic, space group $P2_1/c$, with $a = 6.566$ (1) Å, $b = 8.483$ (1) Å, $c = 7.140$ (1) Å, $\beta = 115.25°$, and $Z = 4$. Ti–O coordination distances in the new KTP isostructures do not deviate significantly from those in KTP or KTA. Second harmonic generation intensities measured at 532 nm show that optical nonlinearity in NaTP and AgTP is significantly attenuated from that in KTP and NaTA. These results are accounted for by (1) differences in interactions between K, Na, Ag, and the titanyl oxygen atoms, which influence the mixing of a delocalized excited state into the ground-state bonding and nonbonding framework orbitals, and (2) a decrease in bandgap due to the increased basicity of the oxygen atoms in the arsenate derivatives.

1. Introduction

Potassium titanyl phosphate ($KTiOPO_4$, or KTP) has enjoyed considerable success as a nonlinear optical medium for second harmonic generation (SHG) at 1064 nm due to the high-power conversion efficiencies, high damage threshold, large angular acceptance,[1] and the low sensitivity of its phase matching condition to temperature.[2] Both sum-frequency generation (SFG)[3] and optical parametric

* Author to whom correspondence should be addressed.
† Sandia National Laboratories.
‡ University of California.
§ E. I. du Pont de Nemours.

(1) Fan, T. Y.; Huang, C. E.; Hu, B. Q.; Eckhardt, R. C.; Fan, Y. X.; Byer, R. L.; Feigelson, R. S. *Appl. Opt.* **1987**, *26*, 2391.
(2) Zumsteg, F. C.; Bierlein, J. D.; Gier, T. E. *J. Appl. Phys.* **1976**, *47*, 4980.

0897-4756/92/2804-0222$03.00/0 © 1992 American Chemical Society